Numerical study of Vlasov-Poisson equations in the simulation for infinite homogeneous stellar systems

Yingda Cheng * Irene M. Gamba †

April 7, 2011

Dedicated to Professor Philip J. Morrison on the occasion of his 60th birthday.

Abstract

In this paper, we consider the gravitational Vlasov-Poisson (VP), or the so-called collisionless Boltzmann-Poisson equations for the self-gravitating collisionless stellar systems. We compute the solutions using a high-order discontinuous Galerkin method for the Vlasov equation and the exact method for the Poisson equation in the one-dimensional setting. The wavenumbers are taken to be greater than or less than the Jeans wavenumber, through which we include the case of both damping and Jeans instability. The method is shown to be stable, accurate and conservative. We pay particular attentions to the BGK modes, as well as the behaviors of the solutions associated with various wavenumbers.

Keywords: Jeans instability, Vlasov-Poisson, collisionless Boltzmann, discontinuous Galerkin methods, positivity-preserving.

1 Introduction

In this paper, we consider the gravitational Vlasov-Poisson (VP), or the so-called collisionless Boltzmann-Poisson equations for the self-gravitating collisionless stellar systems. The VP system in this case describes the evolution of the density of stars in phase space and is given as follows [4, 5],

$$\begin{aligned} \partial_t f + v\cdot\nabla_x f + E\cdot\nabla_v f = 0 \qquad & \Omega\times(0,T] \\ \Delta_x\Phi = 4\pi G\rho_0(\int_{\mathbb{R}^n} f dv - 1) \qquad & \Omega_x\times(0,T] \\ E = -\nabla_x\Phi \qquad & \Omega_x\times(0,T] \end{aligned} \tag{1}$$

*Department of Mathematics and ICES, University of Texas at Austin Austin, TX 78712 U.S.A. ycheng@math.utexas.edu. Phone: 1-512-232-7761. Fax: 1-512-471-8694.

†Department of Mathematics and ICES, University of Texas at Austin Austin, TX 78712 U.S.A. gamba@math.utexas.edu. Phone: 1-512-471-7422. Fax: 1-512-471-8694.

Here f is the stellar distribution function, G is the gravitational constant, ρ_0 is the density of the infinite homogeneous medium, E is the gravitational field, and the constant -1 in the total charge for the Poisson equation denotes the cosmological background density. The domain $\Omega = \Omega_x \times \mathbb{R}^n$, where Ω_x is the physical space and the phase space is taken to be $\mathbb{R}^n$. More detailed discussions of the above system for the galactic dynamics can be found in the book by Binney and Tremaine [4, 5].

The VP equation (1) conserves the mass, momentum, energy, entropy, enstrophy and total energy of the system. More importantly, if the initial f is a perturbation around the Maxwellian equilibrium distribution

$$f_{eq} = \frac{\rho_0}{(2\pi\sigma^2)^{n/2}} e^{-\frac{1}{2}v^2/\sigma^2},$$

then by *Jeans swindle* after Sir James Jeans, one can obtain the *Jeans wavenumber*

$$k_J = (4\pi G\rho_0/\sigma^2)^{1/2}$$

and the *Jeans length* $\lambda_J = 2\pi/k_J$. For any initial state $f(x, v, 0) = f_{eq}(1 + A \cdot p(kx))$ as a $k-$periodic, zero-averaged, analytic perturbation of the equilibrium state, if $\lambda > \lambda_J$ or $k < k_J$, the perturbation is unstable and the phenomenon is called the *Jeans instability*. Damping of the perturbation should occur only at wavelengths smaller than the Jeans length. This behavior differs significantly from the electrostatic VP equations for collisionless plasmas, where damping should be expected for all wavenumbers under suitable assumptions on the equilibrium velocity profile, for which the Debye length is roughly defined in the same way as the Jeans length [21]. The Jeans instability accounts for the solutions of the VP system that are interpreted as the collapse of interstellar gas clouds and subsequent star formation. In this paper, we will perform a numerical study of (1) with perturbations associated with various wavenumber k for the classical Maxwellian equilibrium.

The VP system with the electrostatic force has been studied extensively for the simulation of collisionless plasmas. Popular numerical approaches include the Particle-In-Cell (PIC) methods [6, 19], the Lagragian particle methods [3], the semi-Lagragian methods [8, 27] and the Eulerian approaches [35, 15], among many others. The Eulerian solvers can achieve high order accuracy with high order schemes. The disadvantage is for systems in high dimensions computational cost will increase dramatically. It is also nontrivial how to conserve the physical quantities and the positivity of numerical solutions at the same time. For the gravitational case, semi-Lagragian schemes by Cheng and Knorr [8] have been used to simulate one-dimensional problems[16], spherical stellar systems [17] and stellar disks [22]. An Eulerian code has been used to compute the gravitational collapse of a one-dimensional system in [28].

In this paper, we propose to use discontinuous Galerkin methods to solve the VP system (1). The original DG method dates back to 1973, and was introduced by Reed and Hill [24] for neutron transport. Lesaint and Raviart [20] performed the first convergence study for the original DG method. Cockburn and Shu in a series of papers [13, 12, 11, 10, 14] developed the Runge-Kutta DG (RKDG) method for hyperbolic equations. The DG methods have been used to simulate the VP system in plasmas [18] and some theoretical aspects are discussed in

[1, 2]. Our current work uses a maximum-principle-satisfying limiter that has been recently proposed by Zhang *et al.* in [30] for conservation laws on cartesian meshes, and later extended on triangular meshes [34]. This limiter has been used to develop positivity-preserving schemes for compressible Euler [31, 33], shallow water equations [29], Vlasov-Boltzmann transport equations [9]. It has also been employed recently in the framework of semi-Lagragian DG methods [25, 23]. The resulting scheme preserves positivity of numerical solution and is genuinely high order accurate for arbitrary order of discretization. For a complete review for this method, one can refer to [32].

The rest of the paper is organized as follows: in Section 2, we describe the numerical algorithm. Section 3 is devoted to the simulation results for the case of damping and Jeans instability, respectively. We conclude and provide future work in Section 4.

2 Numerical methods

In this section, we will introduce our numerical approach. We will focus on the one-dimensional case in our discussion. For simplicity, the VP system (1) is renormalized as

$$\begin{aligned} \partial_t f + v \cdot \nabla_x f + E \cdot \nabla_v f = 0 \qquad & \Omega \times (0,T] \\ \Delta_x \Phi = \int_{\mathbb{R}^n} f dv - 1 \qquad & \Omega_x \times (0,T] \\ E = -\nabla_x \Phi \qquad & \Omega_x \times (0,T] \end{aligned} \tag{2}$$

and without loss of generality, we consider the Maxwellian equilibrium distribution

$$f_{eq} = \frac{1}{\sqrt{2\pi}} e^{-\frac{1}{2}v^2}.$$

Consequently, the Jeans wavenumber is $k_J = 1$. The domain we consider is $\Omega = [0, L] \times [-V_c, V_c]$, where V_c is chosen large enough and may be different for various test cases. The boundary conditions in the $x-$direction has been assumed to be periodic. The domain Ω is partitioned as follows

$$0 = x_{\frac{1}{2}} < x_{\frac{3}{2}} < \ldots < x_{N_x+\frac{1}{2}} = L, \qquad -V_c = v_{\frac{1}{2}} < v_{\frac{3}{2}} < \ldots < v_{N_v+\frac{1}{2}} = V_c.$$

The computational cells are defined as:

$$\begin{aligned} & I_{i,j} = [x_{i-\frac{1}{2}}, x_{i+\frac{1}{2}}] \times [v_{j-\frac{1}{2}}, v_{j+\frac{1}{2}}], \\ & J_i = [x_{i-1/2}, x_{i+1/2}], \quad K_j = [v_{j-1/2}, v_{j+1/2}] \quad i = 1, \ldots N_x, \quad j = 1, \ldots N_v, \end{aligned}$$

where $x_i = \frac{1}{2}(x_{i-\frac{1}{2}} + x_{i+\frac{1}{2}})$, and $v_j = \frac{1}{2}(v_{j-1/2} + v_{j+1/2})$ are center points of the cells.

For all macroscopic quantities, we use the piecewise polynomial space in the $x-$direction

$$Z_h^k = \{\xi : \xi|_{J_i} \in P^k(J_i),\ i = 1, \ldots N_x\}, \tag{3}$$

where $P^k(J_i)$ is the space of polynomials of degree up to k on J_i. For the full (x, v) space, we define

$$V_h^k = \{\varphi : \varphi|_{I_{i,j}} \in \mathbb{P}^k(I_{i,j}),\ i = 1, \dots N_x, \quad j = 1, \dots N_v\} \tag{4}$$

where $\mathbb{P}^k(I_{i,j}) = span\{x^l\, v^m, \forall\, 0 \le l + m \le k, l \ge 0, m \ge 0\}$ on $I_{i,j}$.

We start by reviewing the semi-discrete DG scheme formulation for the Vlasov equation. We find $f_h(x,t) \in V_h^k$, such that

$$\begin{aligned}
&\int_{I_{i,j}} (f_h)_t \varphi_h dx dv - \int_{I_{i,j}} v f_h (\varphi_h)_x dx dv + \int_{K_j} (\widehat{v f_h} \varphi_h^-)_{i+1/2,v} dv - \int_{K_j} (\widehat{v f_h} \varphi_h^+)_{i-1/2,v} dv \\
&- \int_{I_{i,j}} E_h f_h (\varphi_h)_v dx dv - \int_{J_i} (\widehat{E_h f_h} \varphi_h^-)_{x,j+1/2} dx + \int_{J_i} (\widehat{E_h f_h} \varphi_h^+)_{x,j-1/2} dx = 0
\end{aligned} \tag{5}$$

holds for any test function $\varphi_h(x,t) \in V_h^k$. Here and below, We use the following notations $(\varphi_h)^{\pm}_{i+1/2,v} = \lim_{\epsilon \to 0} \varphi_h(x_{i+1/2} \pm \epsilon, v)$, and $(\varphi_h)^{\pm}_{x,j+1/2} = \lim_{\epsilon \to 0} \varphi_h(x, v_{j+1/2} \pm \epsilon)$. $\widehat{v f_h}$ are numerical fluxes. We can assume that in each K_j, v holds constant sign by properly partitioning the mesh. We can then use the upwind flux, which is defined as

$$\widehat{v f_h} = \begin{cases} v f_h^- & \text{if} \quad v \ge 0 \quad \text{in} \quad K_j \\ v f_h^+ & \text{if} \quad v < 0 \quad \text{in} \quad K_j \end{cases}. \tag{6}$$

and

$$\widehat{E_h f_h} = \begin{cases} E_h f_h^- & \text{if} \quad \int_{J_i} E_h dx \le 0 \\ E_h f_h^+ & \text{if} \quad \int_{J_i} E_h dx > 0 \end{cases}. \tag{7}$$

The above description coupled with a suitable time discretization, e.g. the TVD Runge-Kutta method [26] will complete the RKDG methods. Next, we will describe the positivity-preserving schemes as summarized in [32].

In each of the forward Euler step of the Runge-Kutta time discretization, the following procedures are performed:

- On each cell $I_{i,j}$, evaluate $T_{i,j} = \min_{(x,v) \in S_{i,j}} f_h(x,v)$, where $S_{i,j} = (S_i^x \bigotimes \hat{S}_j^y) \bigcup (\hat{S}_i^x \bigotimes S_j^y)$, and S_i^x, S_j^y denote the $(k+1)$ Gauss quadrature points, while $\hat{S}_i^x, \hat{S}_j^y$ denote the $(k+1)$ Gauss-Lobatto quadrature points.

- Compute $\tilde{f}_h(x,v) = \theta(f_h(x,v) - (\overline{f_h})_{i,j}) + (\overline{f_h})_{i,j}$, where $(\overline{f_h})_{i,j}$ is the cell average of f_h on $I_{i,j}$, and $\theta = \min\{1, |(\overline{f_h})_{i,j}| / |T_{i,j} - (\overline{f_h})_{i,j}|\}$. This limiter has the effect of keeping the cell average and "squeeze" the function to be positive at points in $S_{i,j}$.

- Use $\tilde{f}_h$ instead of f_h to compute the Euler forward step.

In order to obtain E_h at each time step, we need to solve the Poisson equation numerically. Recall that beyond periodicity, we need to enforce some additional conditions to uniquely

determine Φ. For example, we require $\Phi(0,t) = 0$. In the one-dimensional setting, the exact solution can be then obtained by using the fact that $\Phi(0) = \Phi(L)$ as

$$\Phi_h = \int_0^x \int_0^s \rho_h(z,t)dz\,ds - \frac{x^2}{2} - C_E x,$$

where $C_E = -\frac{L}{2} + \frac{1}{L}\int_0^L \int_0^s \rho_h(z,t)dz\,ds$, and

$$E_h = -(\Phi_h)_x = C_E + x - \int_0^x \rho_h(z,t)dz. \tag{8}$$

From (8), we can see that if $f_h \in V_h^k$, then $\rho_h = \int_{-V_c}^{V_c} f_h dv \in Z_h^k$, hence $E_h \in Z_h^{k+1}$. This approach will be referred to as the "exact" Poisson solver. This formulation is mainly valid in the one-dimensional setting. For multiple-dimensions, a suitable elliptic solver needs to be implemented.

3 Numerical results

In this section, we collect simulation results for (2) with various wavenumbers. The critical Jeans wavenumber in (2) is $k_J = 1$. The initial condition is $f(x,v,0) = f_{eq}(1 + A\cos(kx))$. The computational domain is taken as $x \in [0, L = 2\pi/k], v \in [-V_c, V_c]$. From a classical calculation of the linear theory, we can derive the dispersion relation as

$$\varepsilon(k,\omega) = 1 + \frac{1}{k^2}\{1 + \frac{\omega}{\sqrt{2}k} Z(\frac{\omega}{\sqrt{2}k})\}, \tag{9}$$

where the plasma $Z-$function is defined as

$$Z(z) = \frac{1}{\sqrt{\pi}} \int_{-\infty}^{\infty} e^{-t^2} \frac{dt}{t-z} = 2ie^{-z^2} \int_{-\infty}^{iz} e^{-t^2} dt.$$

This relation will be used to calculate damping or growth rate to benchmark with our numerical results.

3.1 Damping phenomena

In this subsection, we will consider the case of $k/k_J > 1$. We first start with $k/k_J = 2.0$. Here $V_c = 5$ and the perturbation is of magnitude $A = 0.1$. We use P^2 elements and third-order TVD-RK time stepping on a 200×400 mesh. In this case, the damping is very strong. In Figure 1, we plot the time evolution of the Log Fourier amplitude for gravitational field and density. Here, we assume that, the density can be expanded in the Fourier series $\rho_h(x) = \sum_{n\geq 0} \rho_n \cos(nkx)$. The "log Fourier mode" for the gravitational field [18] is defined as $logFM_n(t) = \log_{10}\left(\frac{1}{L}\sqrt{|\int_0^L E_h(x,t)\sin(knx)dx|^2 + |\int_0^L E_h(x,t)\cos(knx)dx|^2}\right)$. The theoretical damping rate from the dispersion relation (9) is -0.187. From Figure 1, we measure the

damping rate for the first mode of density ρ_1 ($0.5 \leq t \leq 3$) to be -0.1872. Unlike ρ_1, $logFM_1$ first goes through an initial growth phase, which makes its damping rate inaccurate. In Figure 2, we plot the evolution of the macroscopic quantities. It was observed that this solver can accurately conserve the particle number, momentum and total energy. Figure 3(a) contains a plot of the BGK mode ($f(x, v, T)$ vs $\epsilon = v^2/2 + \Phi(x, T)$) at $T = 100$. In Figure 3(b), we have seen the system has almost reached at steady state at $T = 100$. In Figures 3(c) and 3(d), we show the details of the BGK plots at $T = 100, 120, 130$. The plots demonstrate an interesting bar type structure with shorter bars near the tail. As time progresses, the height of the bars is reduced (see Figure 3(c)). This verifies the convergence of the BGK modes to a single-valued discrete function as $t \to \infty$. We also remark that the distance between those bars are mesh size dependent, but time independent.

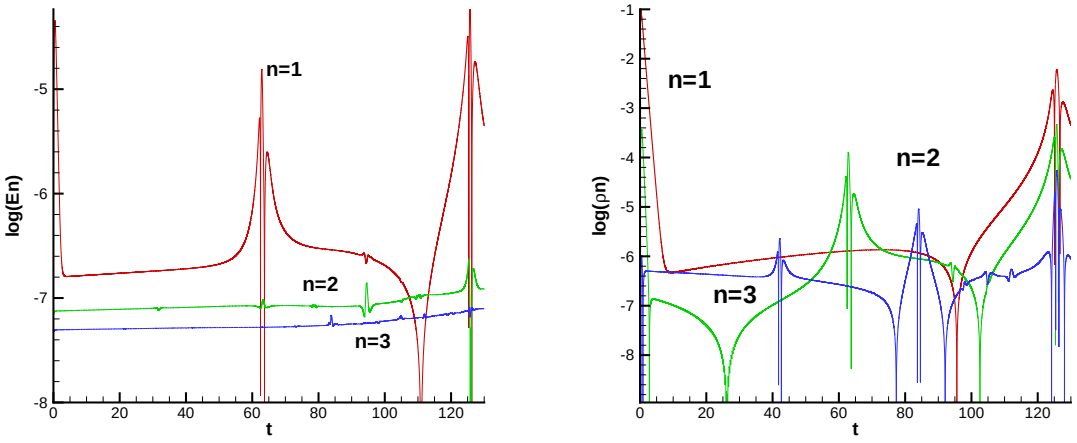

(a) Plot of the first three log Fourier modes ($n = 1, 2, 3$) for the gravitational field $E(x)$ as a function of time

(b) Log Plot of the first three Fourier amplitudes ($n = 1, 2, 3$) for the density $\rho(x)$ as a function of time.

Figure 1: Damping with $k/k_J = 2.0$ and $A = 0.1$. P^2 elements and third-order TVD-RK time stepping on a 200×400 mesh.

Next, we consider $k/k_J = 1.1$, $V_c = 5$, $A = 0.1$. From Figure 4, the numerical damping rate for ρ_1 ($1 \leq t \leq 4$) is -0.1621, while for $logFM_1$ ($1 \leq t \leq 4$) it is -0.1620, which agrees with theoretical rate calculated from the dispersion relation (9), -0.163. In Figure 5, we plot the evolution of the macroscopic quantities. From the momentum plot Figure 6(b), we can identify that the system is close to but not yet at steady state. This fact can seen from the close up plots Figures 6(c) and 6(d), in which detailed structures of the mode can be observed.

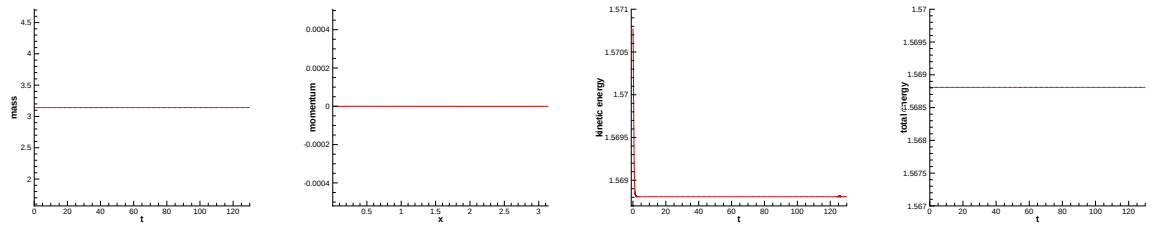

(a) total particle number (b) momentum (c) kinetic energy (d) total energy

Figure 2: Damping with $k/k_J = 2.0$ and $A = 0.1$. Evolution of macroscopic quantities. P^2 elements and third-order TVD-RK time stepping on a 200×400 mesh.

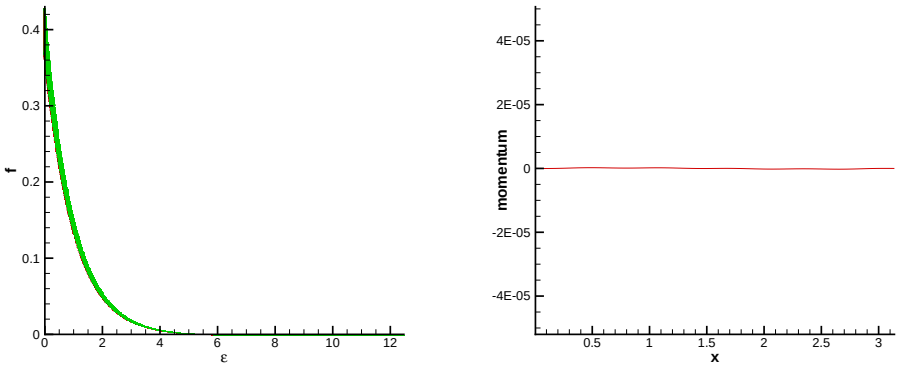

(a) BGK mode at $T = 100$ (b) momentum at $T = 100$

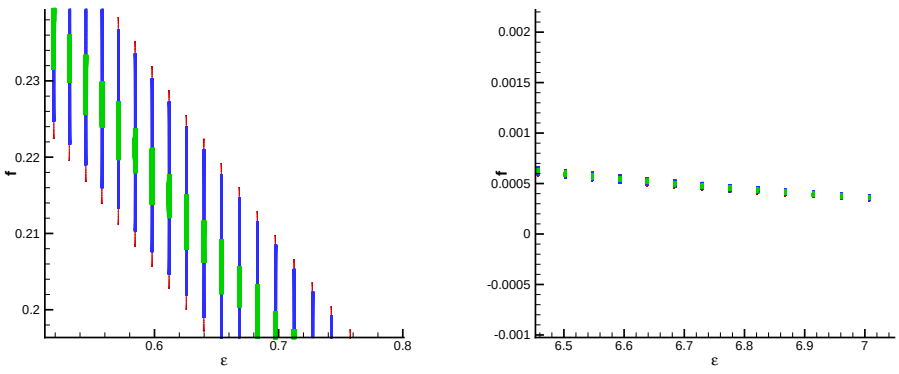

(c) magnified plot of BGK mode at $T = 100, 120, 130$. red: $T = 100$, blue, $T = 120$, green, $T = 130$

(d) magnified plot of BGK mode $T = 100, 120, 130$. red: $T = 100$, blue, $T = 120$, green, $T = 130$

Figure 3: Damping with $k/k_J = 2.0$ and $A = 0.1$. P^2 elements and third-order TVD-RK time stepping on a 200×400 mesh.

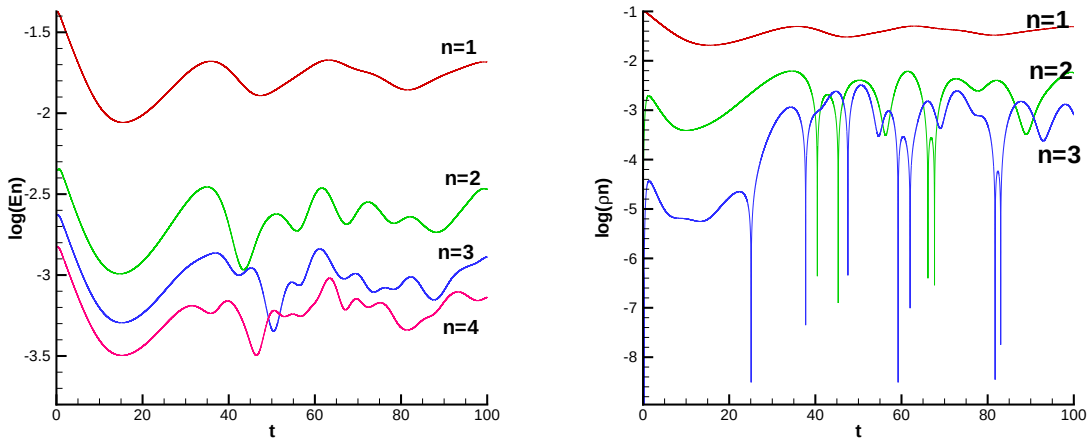

(a) Plot of the first four log Fourier modes ($n = 1, 2, 3, 4$) for the gravitational field $E(x)$ as a function of time

(b) Log Plot of the first three Fourier amplitudes ($n = 1, 2, 3$) for the density $\rho(x)$ as a function of time.

Figure 4: Damping with $k/k_J = 1.1$ and $A = 0.1$. P^2 elements and third-order TVD-RK time stepping on a 200×400 mesh.

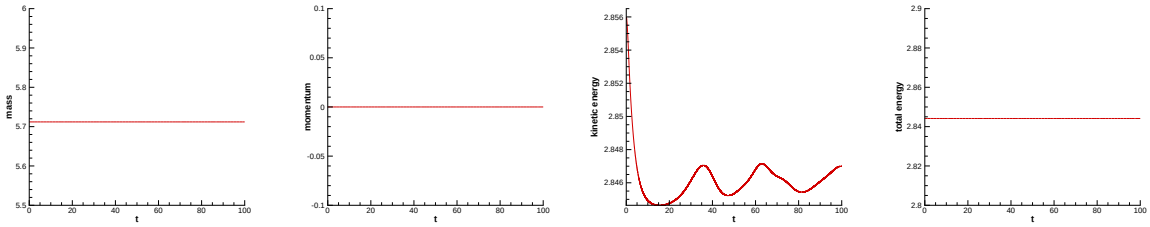

(a) total particle number (b) momentum (c) kinetic energy (d) total energy

Figure 5: Damping with $k/k_J = 1.1$ and $A = 0.1$. Evolution of macroscopic quantities. P^2 elements and third-order TVD-RK time stepping on a 200×400 mesh.

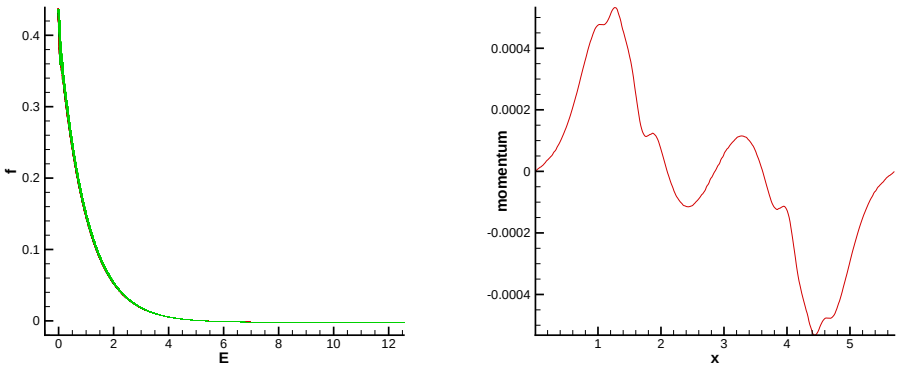

(a) BGK mode (b) momentum

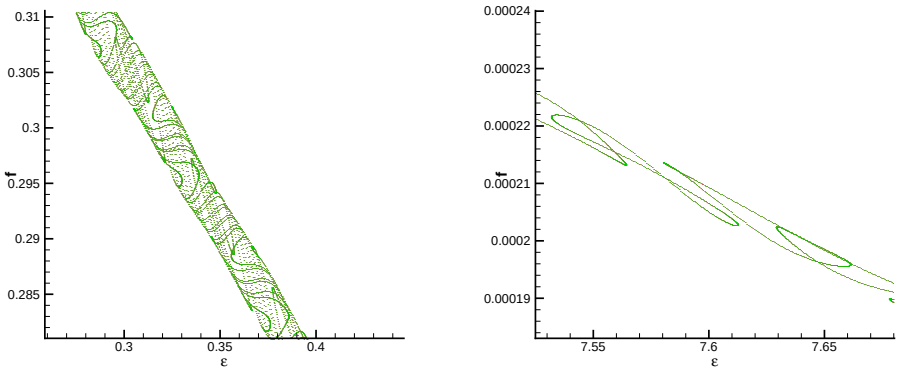

(c) magnified plot of BGK mode (d) magnified plot of BGK mode

Figure 6: Damping with $k/k_J = 1.1$ and $A = 0.1$ at $T = 100$. P^2 elements and third-order TVD-RK time stepping on a 200×400 mesh.

3.2 The Jeans instability

In this subsection, we consider the Jeans instability case with $k/k_J < 1$. First we take $k/k_J = 0.8$, $A = 0.01$, and $V_c = 5$. In Figure 7, we measure the growth rate for ρ_1 $(1 \le t \le 4)$ to be 0.3048 and 0.3051 for $logFM_1$ $(1 \le t \le 4)$. Those agree with theoretical rate from the dispersion relation (9), 0.304. After saturation, we can see that ρ_1 undergoes oscillation that eventually damps. In Figure 8, we observe the conservation of mass, momentum and total energy. In Figure 9(a), we plot the BGK mode at $T = 100$. It clearly does not form a curve because the system is not in equilibrium, see Figure 9(b) for verification. The contour plots of the *pdf* at various times can be found in Figure 10.

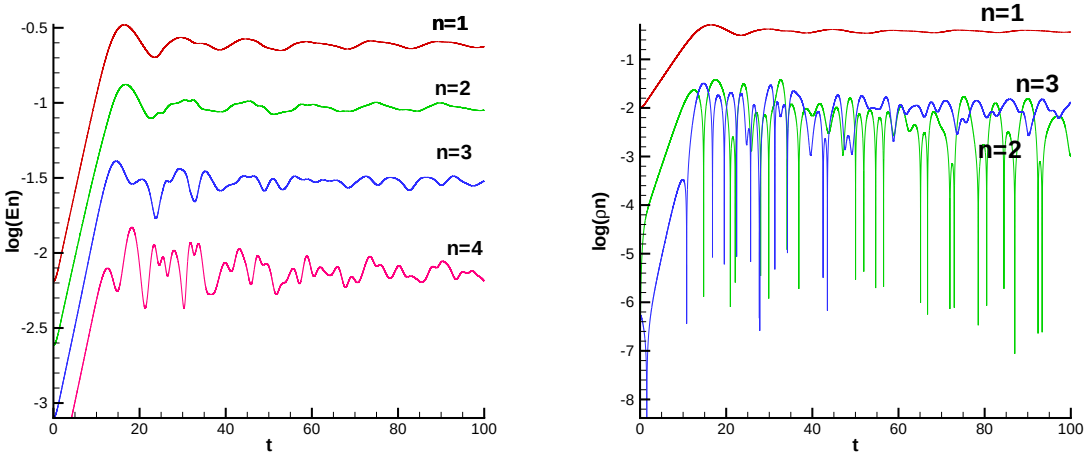

(a) Plot of the first four log Fourier modes $(n = 1, 2, 3, 4)$ for the gravitational field $E(x)$ as a function of time

(b) Log Plot of the first three Fourier amplitudes $(n = 1, 2, 3)$ for the density $\rho(x)$ as a function of time.

Figure 7: Jeans instability with $k/k_J = 0.8$ and $A = 0.01$. P^2 elements and third-order TVD-RK time stepping on a 200×400 mesh.

Next, we consider the case of the strong Jeans instability. Here, $k/k_J = 0.1$, $A = 0.01$, and the domain in v needs to be enlarged to $V_c = 35$. In this problem, unlike all previous cases, the total energy is not well conserved with the positivity-preserving limiter. We believe this is due to the strong instability of the problem. We choose to use the RKDG scheme without the positivity-preserving limiter only for this example. From Figure 11, the growth rate for ρ_1 $(2 \le t \le 4)$ is 0.9764, for $logFM_1$ $(1 \le t \le 4)$ is 0.9756, which agrees with theoretical rate from the dispersion relation (9), 0.985. The contour plots can be found in Figures 12. The distribution is first distorted and then develops a core-halo structure similar to the corresponding one in [16] for the same choice of wavenumber and amplitude of perturbation.

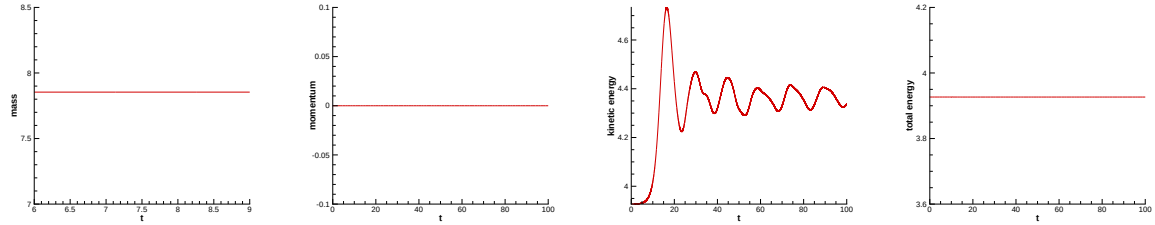

(a) total particle number (b) momentum (c) kinetic energy (d) total energy

Figure 8: Jeans instability with $k/k_J = 0.8$ and $A = 0.01$. Evolution of macroscopic quantities. P^2 elements and third-order TVD-RK time stepping on a 200×400 mesh.

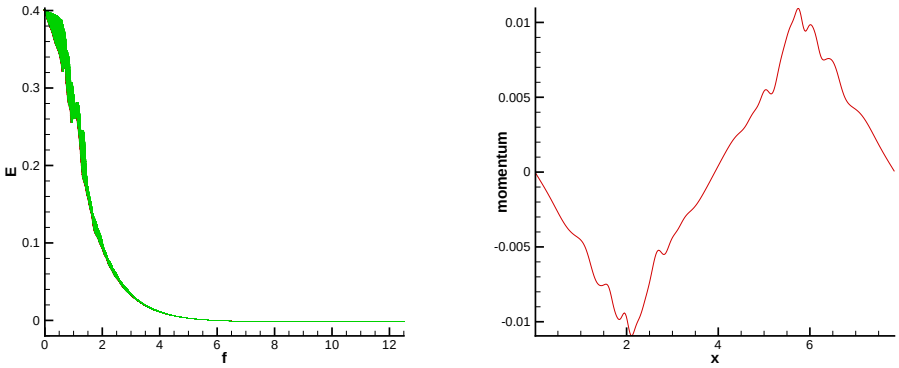

(a) BGK mode (b) momentum

Figure 9: Jeans instability with $k/k_J = 0.8$ and $A = 0.01$. $T = 100$. P^2 elements and third-order TVD-RK time stepping on a 200×400 mesh.

4 Conclusions and future work

In this paper, we use a high-order discontinuous Galerkin scheme to compute the gravitational Vlasov-Poisson equations. The scheme is stable, accurate and conservative. We compute the case of damping and the Jeans instability with the initial condition taken as a perturbation of the Maxwellian distribution. Future work includes a detailed study of the Jeans instability with multi-bump (two-streaming) distributions, and comparison with the fluid theory [7].

Acknowledgments

The authors thank Philip J. Morrison for many helpful and illuminating discussions. Yingda Cheng is supported by grant NSF DMS-1016001. Irene M. Gamba is supported by grant NSF DMS-0807712 and also DMS-0757450. Support from the Institute of Computational

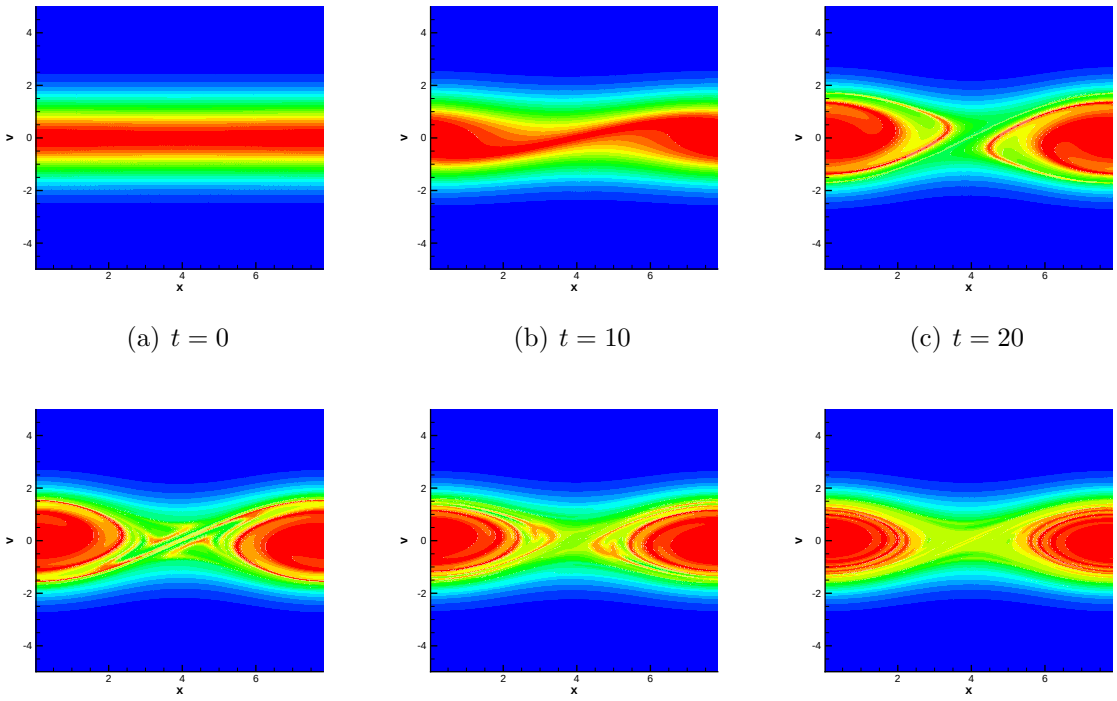

(a) $t = 0$ (b) $t = 10$ (c) $t = 20$

(d) $t = 30$ (e) $t = 50$ (f) $t = 100$

Figure 10: Jeans instability with $k/k_J = 0.8$ and $A = 0.01$. Contour plots of *pdf* at various times. P^2 elements and third-order TVD-RK time stepping on a 200×400 mesh.

Engineering and Sciences and the University of Texas Austin is gratefully acknowledged.

References

[1] B. Ayuso, J. A. Carrillo, and C.-W. Shu. Discontinuous Galerkin methods for the one-dimensional Vlasov-Poisson system. 2009. preprint.

[2] B. Ayuso, J. A. Carrillo, and C.-W. Shu. Discontinuous Galerkin methods for the multi-dimensional Vlasov-Poisson problems. 2010. preprint.

[3] J. Barnes and P. Hut. A hierarchical o(n log n) force-calculation algorithm. *Nature*, 324:446–449, 1986.

[4] J. Binney and S. Tremaine. *Galactic dynamics*. Princeton Series in Astrophysics. Princeton University Press, first edition, 1987.

[5] J. Binney and S. Tremaine. *Galactic dynamics*. Princeton Series in Astrophysics. Princeton University Press, second edition, 2008.

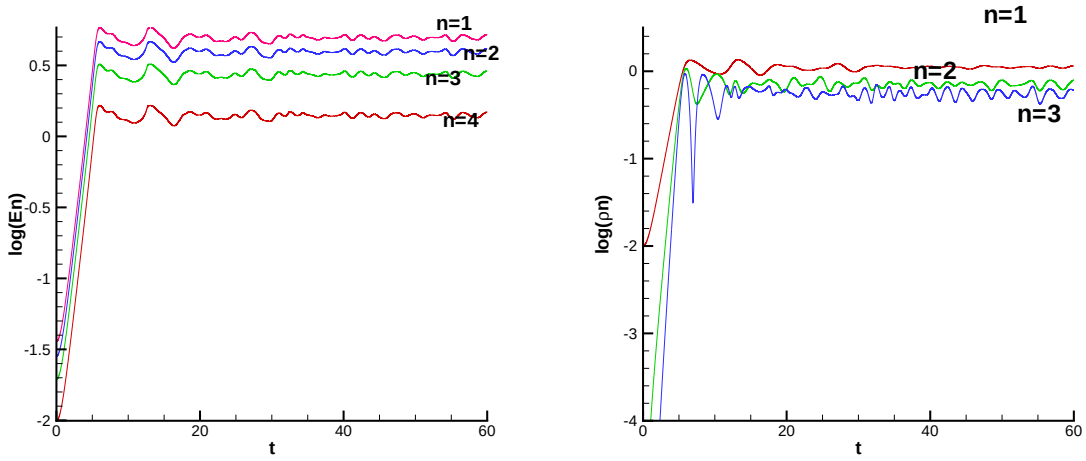

(a) Plot of the first three log Fourier modes ($n = 1, 2, 3$) for the gravitational field $E(x)$ as a function of time

(b) Log Plot of the first three Fourier amplitudes ($n = 1, 2, 3$) for the density $\rho(x)$ as a function of time.

Figure 11: Jeans instability with $k/k_J = 0.1$ and $A = 0.01$. P^2 elements and third-order TVD-RK time stepping on a 200×400 mesh.

[6] C. K. Birdsall and A. B. Langdon. *Plasma physics via computer simulation*. Institute of Physics Publishing, 1991.

[7] A. Casti, P. J. Morrison, and E. A. Spiegel. Negative energy modes and gravitational instability of interpenetrating fluids. *Annals of the New York Academy of Sciences*, 867:93C108, 1998. in Nonlinear Dynamics and Chaos in Astrophysics, eds. J. R. Buchler, S. T. Gottesman, and H. E. Kandrup.

[8] C. Z. Cheng and G. Knorr. The integration of the Vlasov equation in configuration space. *Journal of Computational Physics*, 22(3):330–351, 1976.

[9] Y. Cheng, I. Gamba, and J. Proft. Positivity-preserving discontinuous Galerkin schemes for linear Vlasov-Boltzmann transport equations. *Math. Comp.*, 2010. to appear.

[10] B. Cockburn, S. Hou, and C.-W. Shu. The Runge-Kutta local projection discontinuous Galerkin finite element method for conservation laws IV: the multidimensional case. *Math. Comput.*, 54:545–581, 1990.

[11] B. Cockburn, S. Y. Lin, and C.-W. Shu. TVB Runge-Kutta local projection discontinuous Galerkin finite element method for conservation laws III: one dimensional systems. *J. Comput. Phys.*, 84:90–113, 1989.

[12] B. Cockburn and C.-W. Shu. TVB Runge-Kutta local projection discontinuous Galerkin finite element method for conservation laws II: general framework. *Math. Comput.*, 52:411–435, 1989.

[13] B. Cockburn and C.-W. Shu. The Runge-Kutta local projection p1-discontinuous Galerkin finite element method for scalar conservation laws. *Math. Model. Num. Anal.*, 25:337–361, 1991.

[14] B. Cockburn and C.-W. Shu. The Runge-Kutta discontinuous Galerkin method for conservation laws V: multidimensional systems. *J. Comput. Phys.*, 141:199–224, 1998.

[15] F. Filbet and E. Sonnendrücker. Comparison of Eulerian Vlasov solvers. *Computer Physics Communications*, 150:247–266, 2003.

[16] T. Fujiwara. Vlasov simulations of stellar systems: infinite homogeneous case. *ASTRON. SOC. OF JAPAN. PUBLICATIONS*, 33:531–540, 1981.

[17] T. Fujiwara. Integration of the collisionless Boltzmann equation for spherical stellar systems. *ASTRON. SOC. OF JAPAN. PUBLICATIONS*, 35:547–558, 1983.

[18] R. E. Heath, I. M. Gamba, P. J. Morrison, and C. Michler. A discontinuous Galerkin method for the Vlasov-Poisson system. *J. Comp. Phys.*, 2011. to appear.

[19] R. W. Hockney and J. W. Eastwood. *Computer simulation using particles*. McGraw-Hill, New York, 1981.

[20] P. Lesaint and P.-A. Raviart. On a finite element method for solving the neutron transport equation. In *Mathematical aspects of finite elements in partial differential equations (Proc. Sympos., Math. Res. Center, Univ. Wisconsin, Madison, Wis., 1974)*, pages 89–123. Math. Res. Center, Univ. of Wisconsin-Madison, Academic Press, New York, 1974.

[21] C. Mouhot and C. Villani. On Landau damping. *Acta Mathematica*, 2009. to appear.

[22] M. T. Nishida, Y. Watanabe, T. Fujiwara, and S. Kato. Collisionless Boltzmann simulation of stellar disks: III deformation of spiral normal modes to bar patterns. *ASTRON. SOC. OF JAPAN. PUBLICATIONS*, 36:27–40, 1984.

[23] J.-M. Qiu and C.-W. Shu. Positivity preserving semi-Lagrangian discontinuous Galerkin formulation: theoretical analysis and application to the Vlasov-Poisson system. 2011. submitted to J. Comp. Phys.

[24] W. Reed and T. Hill. Tiangular mesh methods for the neutron transport equation. Technical report, Los Alamos National Laboratory, Los Alamos, NM, 1973.

[25] J. Rossmanith and D. Seal. A positivity-preserving high-order semi-Lagrangian discontinuous Galerkin scheme for the Vlasov-Poisson equations. 2011. submitted to J. Comp. Phys.

[26] C.-W. Shu and S. Osher. Efficient implementation of essentially non-oscillatory shock-capturing schemes. *J. Comput. Phys.*, 77:439–471, 1988.

[27] E. Sonnendrücker, J. Roche, P. Bertrand, and A. Ghizzo. The semi-Lagrangian method for the numerical resolution of the Vlasov equation. *J. Comp. Phys.*, 149(2):201–220, 1999.

[28] R. L. White. A new numerical technique for calculation of phase space evolution of stellar systems. *THE USE OF SUPERCOMPUTERS IN STELLAR DYNAMICS*, 267:167–174, 1986. Lecture Notes in Physics.

[29] Y. Xing, X. Zhang, and C.-W. Shu. Positivity preserving high order well balanced discontinuous Galerkin methods for the shallow water equations. *Advances in Water Resources*, 33:1476–1493, 2010.

[30] X. Zhang and C.-W. Shu. On maximum-principle-satisfying high order schemes for scalar conservation laws. *J. Comput. Phys.*, 229:3091–3120, 2010.

[31] X. Zhang and C.-W. Shu. On positivity preserving high order discontinuous Galerkin schemes for compressible Euler equations on rectangular meshes. *J. Comput. Phys.*, 229:8918–8934, 2010.

[32] X. Zhang and C.-W. Shu. Maximum-principle-satisfying and positivity-preserving high order schemes for conservation laws: Survey and new developments. 2011. submitted to Proceedings of the Royal Society A.

[33] X. Zhang and C.-W. Shu. Positivity-preserving high order discontinuous Galerkin schemes for compressible Euler equations with source terms. *J. Comput. Phys.*, 230:1238–1248, 2011.

[34] X. Zhang, Y. Xia, and C.-W. Shu. Maximum-principle-satisfying and positivity-preserving high order discontinuous Galerkin schemes for conservation laws on triangular meshes. *J. Sci. Comp.* to appear.

[35] T. Zhou, Y. Guo, and C.-W. Shu. Numerical study on Landau damping. *Physica D: Nonlinear Phenomena*, 157(4):322–333, 2001.

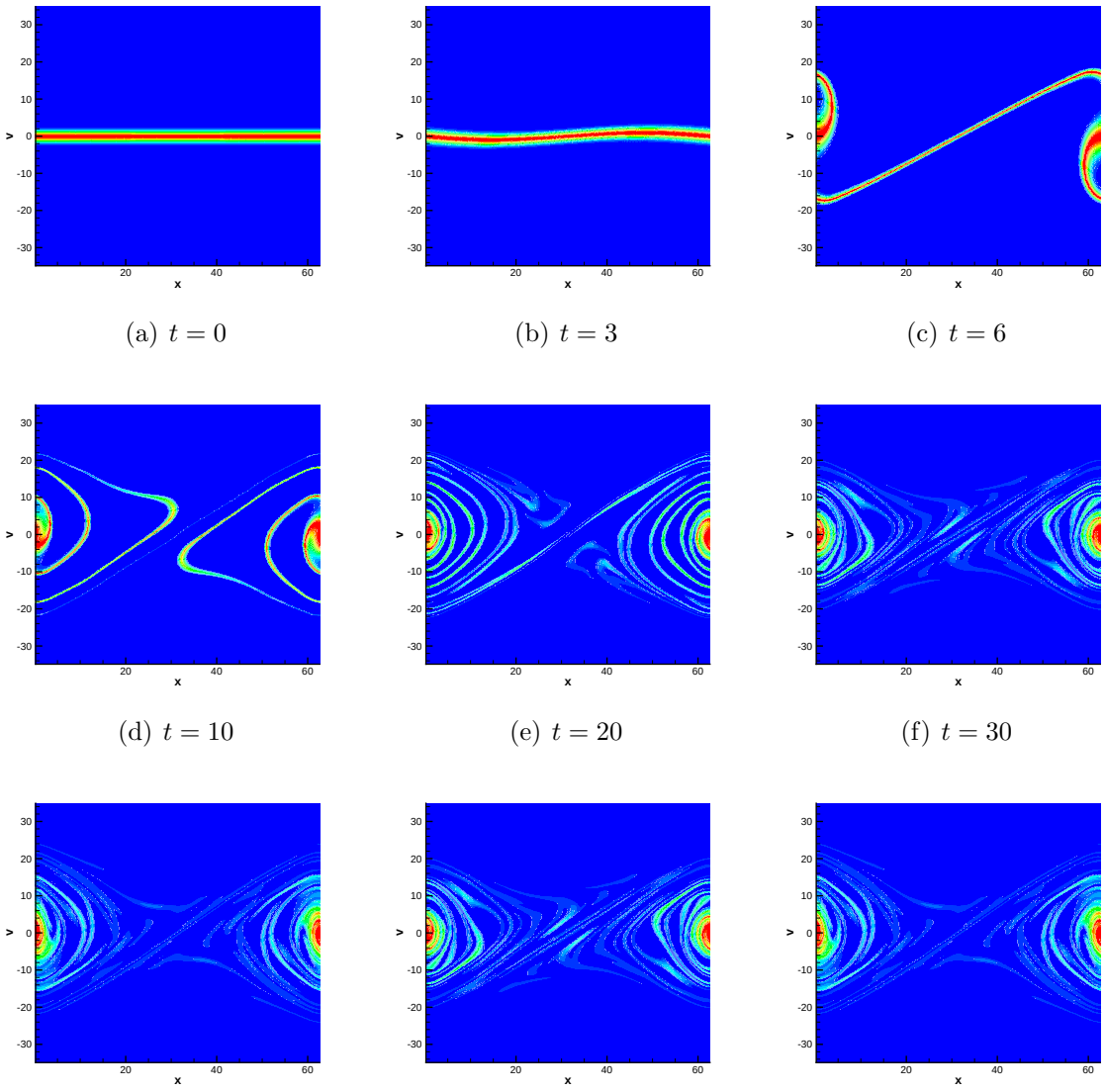

(a) $t = 0$ (b) $t = 3$ (c) $t = 6$

(d) $t = 10$ (e) $t = 20$ (f) $t = 30$

(g) $t = 40$ (h) $t = 50$ (i) $t = 60$

Figure 12: Jeans instability with $k/k_J = 0.1$ and $A = 0.01$. Contour plots of *pdf* at various times. P^2 elements and third-order TVD-RK time stepping on a 200×400 mesh.